Algorithm Theoretical Basis Document of aerosol by non-polarization for GCOM-C/SGLI

2020.05　Mayumi Yoshida

Table of Contents

1. Introduction

Aerosols influence the energy budget of the earth's climate system through scattering and absorbing solar radiation. For a more precise estimation of the impact of aerosols on climate systems, investigation of the behavior of aerosols on a global scale is essential but challenging because aerosol amounts and characteristics vary over space and time.

The multiple uses of various imaging sensors on both geostationary and polar-orbiting satellites are helpful to understand a complete picture of aerosol distribution in the global scale. The common algorithm for various sensors over different ground targets (ocean/land) provides more consistent aerosol retrievals over the globe than independent algorithms. Therefore we developed a common retrieval algorithm of the aerosol optical properties to various satellite sensors (Yoshida et al., 2018) based on the method developed by Higurashi and Nakajima (1998) and Fukuda et al. (2013). This approach was applied to GCOM-C/SGLI non-polarization channels.

In addition, aerosol data assimilation studies using satellite data have also been developed to obtain better initial conditions for the aerosol transport model. Since not all parameters can be accurately detected by satellite sensors, and

unrealistic assumptions of aerosol parameters are a major cause of retrieval errors, adding the model information is expected to improve the retrieval accuracy.

In Version2 algorithm, we utilize the forecast of an aerosol transport model for a priori estimates of the retrieval (Yoshida et al., 2020). This allows the aerosol information in the aerosol transport model to be used for retrieval. And by using the assimilated forecast, information from previous satellite observations can be propagated to future retrievals through the aerosol transport model.

The SGLI channels used for the retrieval are given in section 2. The details of the retrieval methodology is explained in sections 3. Details on the candidate aerosol models and lookup table are described in sections 4 and 5, respectively.

2. Channels for aerosol retrieval by SGLI

The SGLI channels used for the aerosol retrieval are listed on Table 1. Only the channels longer than 800 nm are used for the algorithm over ocean to avoid the influence of water-leaving radiance.

Table 1 Channels of SGLI for aerosol retrieval

CH	center of wavelength[nm]	spatial resolution [m]	ocean	land
VN1	380	250		x
VN2	412			x
VN3	443			x
VN4	490			
VN5	530			x
VN6	565			
VN7	673.5			
VN8	673.5			x
VN9	763	1000		
VN10	868.5	250	x	
VN11	868.5			
SW1	1050	1000	x	
SW2	1380			
SW3	1630	250	x	
SW4	2210	1000	x	

3. Basic principles of the aerosol retrieval algorithm

We developed a common retrieval algorithm to estimate τ, ω, and α from various satellite imagers based on the method developed by Higurashi and Nakajima (1999) and Fukuda et al. (2013). In case of the Lambertian target, the TOA reflectance ρ_i^{sim} at a particular channel *i* can be approximated by:

$$\rho_i^{sim}(\theta_0,\theta,\varphi) = \rho_i^a(\theta_0,\theta,\varphi) + \frac{t_i^s(\theta_0)\cdot t_i^v(\theta)\cdot \rho_i^s(\theta_0,\theta,\varphi)}{1-s_i\cdot\rho_i^s(\theta_0,\theta,\varphi)}, \quad (1)$$

where ρ_i^a is the atmospheric path reflectance, and t_i^s and t_i^v represent total

transmittance, from solar to surface and from surface to sensor, respectively. s_i is the spherical albedo for the illumination of the atmosphere from below, and ρ_i^s is the surface reflectance. Here, θ_0 is the solar zenith angle, θ is the satellite zenith angle, and φ represents the solar/satellite relative azimuth angle. Parameters ($\rho_i^a, t_i^s, t_i^v s_i$) in eq. (1) can be precomputed as a function of geometries ($\theta_0, \theta, and\ \varphi$) for each candidate aerosol model that is defined by the aerosol parameters (τ, external mixing ratio of dry volume concentration for fine particles η_f, and imaginary part of refractive index for fine mode m_i) using a radiative transfer code called System for the Transfer of Atmospheric Radiation whose development was initially lead by the University of Tokyo (STAR, Nakajima and Tanaka 1986, 1988; Stamnes et al. 1988). Additionally, the calculated values are saved as lookup tables. Details on the setting of candidate aerosol models and lookup tables are described in section 4 and 5, respectively.

Figure 1 depicts the flowchart for our algorithm, which estimates three aerosol parameters; namely, τ, η_f, and m_i. Finally, we calculated α and ω by applying the three derived parameters (τ, η_f, and m_i) to the aerosol model that was described in section 4. Here, the spectral dependence of aerosol optical thickness and single scattering albedo is assumed in the candidate aerosol

model by setting the aerosol parameters, such as size distribution and refractive index.

In the retrieval process, we initially calibrated the observed TOA reflectance using the vicarious calibration coefficient "kv0(MOBY+BOUSSOLE)" recommended in JAXA SGLI site (https://suzaku.eorc.jaxa.jp/GCOM_C/data/prelaunch/index_cal.html). Then we selected the clear-sky (i.e., cloud-free) pixel using a cloud detection algorithm developed for GOSAT/CAI, GCOM-C/SGLI, and EarthCARE/MSI (Ishida and Nakajima 2009; Ishida et al. 2011). Further, we corrected the observed TOA reflectance at a channel *i* (ρ_{i}^{obs}) for gas absorption at visible to near-infrared wavelengths. Gas correction was conducted for ozone and water vapor due to their amounts varying significantly with time and location. The corrected TOA reflectance corresponding to the US standard atmosphere ($\rho_{\mathrm{i}}^{obs\prime}$) is given by:

$$\rho_{\mathrm{i}}^{obs\prime} = \frac{T_i^{O_3(USS)}}{T_i^{O_3(OMI)}} \cdot \frac{T_i^{H_2O(USS)}}{T_i^{H_2O(\mathrm{GANAL})}} \cdot \rho_{\mathrm{i}}^{obs}, \qquad (2)$$

where $\mathrm{T}_{\mathrm{i}}^{\mathrm{O}_3(\mathrm{OMI})}$ and $T_i^{H_2O(GANAL)}$ are the transmission factors for ozone and water vapor at the observation points, respectively, and $\mathrm{T}_{\mathrm{i}}^{\mathrm{O}_3(\mathrm{USS})}$ and $T_i^{H_2O(USS)}$ are the transmission factors for the US standard atmosphere, respectively. We used the total ozone columns from JMA chemical transport model and the column water

vapor obtained from JMA global analysis (GANAL) data. Transmission factors $T_i^{O_3}$ and $T_i^{H_2O}$ were pre-calculated for various total ozone columns (*O*) and column water vapor (*w*). Subsequently, coefficients $K_i^{O_3}$, $K_{i,1}^{H_2O}$,$K_{i,2}^{H_2O}$, and $K_{i,3}^{H_2O}$ were derived from the fitting of eqs. (3) and (4) based on the MODIS Algorithm Theoretical Basis Document for Collection 005 and 051 (Levy et al. 2007):

$$T_i^{O_3} = \exp(-GK^{O_3}O), \quad (3)$$

$$T_i^{H_2O} = \exp\left(-\exp\left(K_{i,1}^{H_2O} + K_{i,2}^{H_2O}\ln(Gw) + K_{i,2}^{H_2O}(\ln(Gw))^2\right)\right), \quad (4)$$

where the air mass factor (*G*) is a function of the solar (θ_0) and the sensor zenith angle (θ), such that:

$$G = \frac{1}{\cos(\theta_0)} + \frac{1}{\cos(\theta)}. \quad (5)$$

Next, we derived the aerosol parameters ($\tau, \eta_f,$ and m_i) using an optimal estimation method (Rodgers 2000). The state vector of a set of aerosol parameters $\boldsymbol{x} = \{\tau, \eta_f, m_i\}$ was derived by minimizing the object function *J* (Eq. 6). It uses the measurement vector of a gas-corrected observed reflectance set $\boldsymbol{R} = \{\rho_i^{obs\prime}, i = 1, \ldots, N\}$ and simulated TOA reflectance $\boldsymbol{F(x)} = \{\rho_i^{sim}, i = 1, \ldots, N\}$ that is calculated using eq.(1), where N is the channel number.

$$J = [\boldsymbol{R} - \boldsymbol{F}(\boldsymbol{x})]^T \boldsymbol{S_e^{-1}} [\boldsymbol{R} - \boldsymbol{F}(\boldsymbol{x})] + [\boldsymbol{x} - \boldsymbol{x_a}]^T \boldsymbol{S_a^{-1}} [\boldsymbol{x} - \boldsymbol{x_a}] \quad (6),$$

where $\boldsymbol{x_a} = \{\tau_a, \eta_{f_a}, m_{i_a}\}$ is the vector of a prior estimate of $\boldsymbol{x}$, and $\boldsymbol{S_e}$ and $\boldsymbol{S_a}$ are the covariance matrices of $\boldsymbol{R}$ and $\boldsymbol{x_a}$, respectively. The $\boldsymbol{S_e}$ is given as:

$$\boldsymbol{S_e} = \begin{bmatrix} {\sigma_1}^2 & & 0 \\ & \ddots & \\ 0 & & {\sigma_N}^2 \end{bmatrix}, \qquad (7)$$

where σ_i is the uncertainty in TOA reflectance. Since σ_i is mainly induced from sensor noise (σ_n) and uncertainty in the estimated target land/ocean-surface reflectance ($\Delta\rho_i^s$), we estimate σ_i using eq. (8), as follows:

$$\sigma_i^2 = \sigma_s^2 + \sigma_n^2, \qquad (8)$$

where σ_s is the uncertainty in the TOA reflectance that results from $\Delta\rho_i^s$. We assume $\Delta\rho_i^s$ to be some percentage of the surface reflectance (ρ_i^s) at each channel. We then apply canonical correlation analysis to find the optimal coordinate system, and converted $\boldsymbol{R}$, $\boldsymbol{F(x)}$, and $\boldsymbol{S_e}$ to the coordinate system whose dimension is reduced to the number of retrieved parameters (three).

In the Version1 algorithm, we used spatially and temporally constant values of $\boldsymbol{x_a}$, and $\boldsymbol{S_a}$ that are derived from climate analysis, and assumed that the non-diagonal component of covariance matrices was set to 0 (Yoshida et al. 2018). In the Version2 algorithm, to introduce more realistic a prior estimate and covariance into the retrieval process, we employ the forecast from aerosol assimilation system of the Advanced Himawari Imager (AHI) onboard Himawari-8 instead of the constants (Yoshida et al.,2020). In the Himawari-8/AHI aerosol assimilation system, Level3 aerosol optical thickness from

Himawari-8/AHI (Kikuchi et al., 2018) is assimilated into a global aerosol transport model by the 2D-Var assimilation system (Yumimoto et al. 2018). For the aerosol transport model, we use MASINGAR (Model of Aerosol Species IN the Global AtmospheRe; Tanaka et al. 2003; Tanaka and Chiba 2005) developed at the Meteorological Research Institute (MRI) of the Japan Meteorological Agency (JMA). MASINGAR covers the major tropospheric aerosol components (i.e., black and organic carbon, mineral dust (10-size bins), sea salt (10-size bins), sulfate aerosols)) and their precursors (e.g., sulfur dioxide (SO2), dimethyl sulfide, terpenes)), and is coupled online with an atmospheric general circulation model (MRI-AGCM3; Yukimoto et al. 2012). The detailed method to calculate $\boldsymbol{x}_a$, and $\boldsymbol{S}_a$ from the aerosol assimilation system are described in Yoshida el al., 2020. Finally, the optimal solution of $\boldsymbol{x}$ that minimizes J (Eq. 6) was searched by Levenberg-Marquardt Method.

The uncertainties of the three aerosol parameters (τ, η_f, and m_{i}) $\mathbf{S}_{\hat{\mathbf{x}}}$ were calculated using the law of error propagation, as follows:

$$\boldsymbol{S}_{\hat{\mathbf{x}}} = (\boldsymbol{A}^T \mathbf{S}_{\mathbf{e}}^{-\mathbf{1}} \mathbf{A})^{-1}, \qquad (9)$$

where $\boldsymbol{A}$ is the Jacobian matrix, and $\boldsymbol{S}_{\mathbf{e}}$ is same as in eq. (7), whose elements are calculated using eq. (8). The three aerosol parameters (τ, η_f, and m_{i}), for

which the uncertainties exceeded a threshold value, were treated as invalid values.

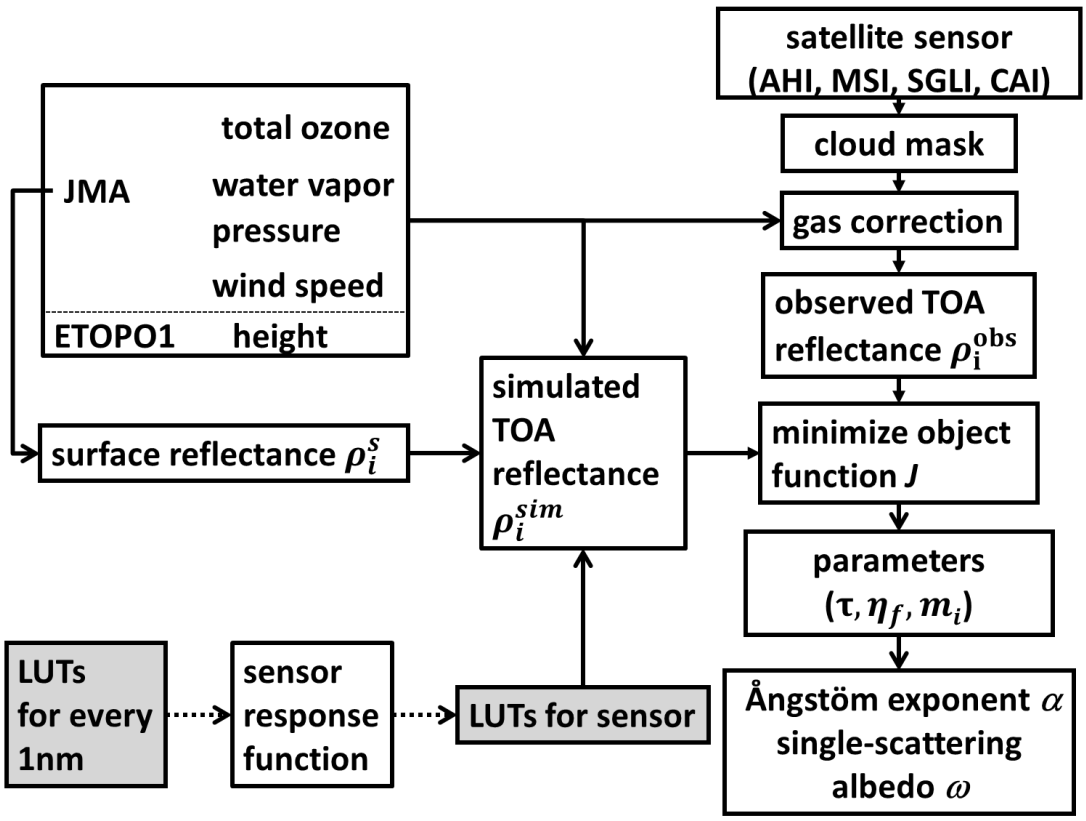

Fig. 1 Flowchart illustrating the retrieval algorithm for L2 aerosol optical properties.

4. Aerosol models

We used common candidate aerosol models over both land and ocean to retrieve aerosols consistently over land and ocean. The candidate aerosol models included aerosol types that were dominant over both ocean and land, and an optimum model was automatically selected. We assumed that the

aerosol model was an external mixture of fine and coarse particles (η_f is the external mixing ratio of the dry volume concentration of fine particles). We set the fine aerosol model based on the average properties of the fine mode for category 1–6 by Omar et al. (2005), which provide the global aerosol models using Aerosol Robotic Network (AERONET) (Holben et al. 1998) measurements. For the coarse aerosol model, we set the external mixture of the pure marine aerosol on the basis of the model that was illustrated by Sayer et al. (2012) and a dust model based on the coarse model of category 1 (dust) that was illustrated by Omar et al. (2005). We define η_c^{dst} as the external mixing ratio of the dry volume concentration of dust particles for the coarse model. Regarding each aerosol size of the fine and coarse models, we used a monomodal lognormal volume size (r_d) distribution, which is as follows:

$$\frac{dV(r_d)}{d\ln r_d} = \frac{C_v}{\sqrt{2\pi}\ln\sigma}\exp\left[-\frac{(\ln r_d - \ln r_v)^2}{2\ln^2\sigma}\right], \quad (11)$$

where C_v is the particle volume concentration, r_v is the volume median radius, and σ is the standard deviation. r_v is set to 0.143, 2.59, and 2.834 (σ is 1.537, 2.054, and 1.908) for fine, coarse marine, and coarse dust, respectively, based on the observations by Omar et al. (2005) and Sayer et al. (2012). Regarding the aerosol shape, we assumed a spherical model for the fine and coarse marine

model, and a non-spherical model for the coarse dust model. The dust non-spherical parameters were based on a yellow dust model (Nakajima et al. 1989), which employed a semi-empirical theory by Pollack and Cuzzi (1980) with r = 1.1, $x0$ = 7, and G = 10 which are parameters of the nonspherical particle scattering theory defined in the original paper. The aerosol vertical distribution was set to the same distribution that was used for rural (dominant at 0–2 km), sea-spray (below 2 km), and yellow sand (4-8 km), for fine, coarse marine, and coarse dust in the STAR code, respectively. The real part of the refractive index was set to 1.439, 1.362, and 1.452 for fine, coarse marine, and coarse dust, respectively, based on Omar et al. (2005) and Sayer et al. (2012). The imaginary part of the refractive index (m_i) was set to 3.0×10^{-9} and 0.0036 at all wavelengths for coarse marine, and coarse dust, respectively, based on Sayer et al. (2012) and Omar et al. (2005). However, m_i for the fine aerosol model was perturbed to represent a nonabsorbing and absorbing aerosol. To decrease the number of derived parameters, m_i varied with η_c^{dst} such that the fine and coarse models exhibited the same ω at 500 nm.

5. Lookup Table

To perform model simulations, we used a radiative transfer code called STAR. For rapid processing, we adopted the lookup table method (Higurashi and Nakajima 1999). The parameters ($\rho_i^a, t_i^s, t_i^v s_i$) in eq. (1) were precomputed for 29 θ_0 (0.0, 2.5, 5.0…., and 70.0˚), 25 θ (0.0, 2.5, 5.0…., and 60.0˚), 37 φ (0.0, 5.0, 10.0…., and 180.0˚), 2 pressures (1,013 and 616.6 hPa), 8 τ (0.0, 0.1, 0.2, 0.4, 0.8, 1.2, 1.6, and 2.0), 11 m_i for fine mode (η_c^{dst} for coarse mode), and 4 η_f (0.0, 0.33, 0.66, and1.0). We calculated these parameters by the radiative transfer code for every 1 nm from 300 nm to 2500 nm. These high-resolution spectral parameters were then weighted using the response function for each sensor. Thus, we could apply the algorithm to a variety of sensors without recalculation. In this manner, we effectively applied the same algorithm and candidate aerosol models to various satellite sensors.

6. Output

Output for SGLI is aerosol optical thickness, angstrom exponent, single scattering albedo, and QA flag. Table 2 shows the descriptions of the QA flag. A priori used for the retrieval is added to QA_flag's attribute.

Table 2 SGLI QA flag, and Mask for statics

	flag	Results	Mask_for_Statistics				
			AROT_ocean	AROT_land	ARAE_ocean	ARAE_land	ARSSA_land
0	Data Availability	0=Available, 1=Not Available	0	0	0	0	0
1	Land / Water Flag	0=Water, 1=Land	0	0	0	0	0
2	Coastal Flag	0=No, 1=Yes	0	0	0	0	0
3	Cloud Flag	0=Clear, 1=Cloudy	0	0	0	0	0
5,4	Aerosol Optical Thickness Confidence Flag	00=Very Good, 01=Good, 10=Marginal, 11=No Confidence or Fill	1,0	1,0	0	0	0
7,6	Angstrom Exponent Confidence Flag	00=Very Good, 01=Good, 10=Marginal, 11=No Confidence or Fill	0	0	1,0	1,0	0
9,8	Aerosol Single Scattering Albedo Confidence Flag	00=Very Good, 01=Good, 10=Marginal, 11=No Confidence or Fill	0	0	0	0	1,0
10	Sunglint Flag	0=No, 1=Yes	0	0	0	0	0
11	Stray-Light Flag	0=No, 1=Yes	0	0	0	0	0
12	Cloud Shadow Possibility Flag	0=No, 1=Yes	0	0	0	0	0
13	Uncertain Surface Reflectance Flag (Turbid Water, Snow/Ice Covered Surface or Rtoa_obs < Rtoa_Rayleigh)	0=No, 1=Yes	0	0	0	0	0
15,14	Spare		0	0	0	0	0

References

Cox, C., and W. Munk, 1954: Statistics of the sea surface derived from sun glitter, J. Mar. Res., 13, 198–227.

Deepak, A., and H. E. Gerber 1983: Report of the experts meeting on aerosols and their climate effects, WCP-55, World Meteorological Organization, Geneva, 107 pp.

Fukuda, S., Nakajima, T., Takenaka, H., Higurashi, A., Kikuchi, N., Nakajima, T. Y., & Ishida, H.,2013: New approaches to removing cloud shadows and evaluating the 380 nm surface reflectance for improved aerosol optical thickness retrievals from the GOSAT/TANSO - Cloud and Aerosol Imager. Journal of Geophysical Research: Atmospheres, 118(24), 13-520.

Higurashi, A., and T. Nakajima, 1999: Development of a two-channel aerosol retrieval algorithm on a global scale using NOAA AVHRR, J. Atmos. Sci., 56, 924-941.

Holben, B. N., T. F. Eck, I. Slutsker, D. Tanré, J. P. Buis, A. Setzer, E. Vermote, J. A. Reagan, Y. Kaufman, T. Nakajima, F. Lavenu, I. Jankowiak, and A. Smirnov, 1998: A federated instrument network and data archive for aerosol characterization. *Remote Sens. Environ.*, **66**, 1–16.

Ishida, H., and T. Y. Nakajima, 2009: Development of an unbiased cloud detection algorithm for a spaceborne multispectral imager, J. Geophys. Res., 114, D07206, doi:10.1029/2008JD010710.

Ishida, H., T. Y. Nakajima, T. Yokota, N. Kikuchi, and H. Watanabe, 2011: Investigation of GOSAT TANSO-CAI cloud screening ability through an inter-satellite comparison, J. Appl. Meteor. Climatol., 50, 1571–1586. doi:10.1175/2011JAMC2672.1.

Kikuchi M., Murakami, H., Suzuki, K., Nagao, T. M., and Higurashi A.: Improved Hourly Estimates of Aerosol Optical Thickness using Spatiotemporal Variability Derived from Himawari-8 Geostationary Satellite, IEEE Trans. Geosci. Remote Sensing, 2018, doi: 10.1109/TGRS.2018.2800060, 2018.

Levy, R. C., L. A. Remer, S. Mattoo, E. F. Vermote, and Y. J. Kaufman, 2007: Second-generation operational algorithm: Retrieval of aerosol properties over land from inversion of Moderate Resolution Imaging Spectroradiometer

spectral reflectance. *J. Geophys. Res.*, **112**, D13211, doi:10.1029/2006JD007811.

MODIS Algorithm Theoretical Basis Document for Collection 005 and 051: https://modis-atmos.gsfc.nasa.gov/_docs/ATBD_MOD04_C005_rev2.pdf

Nakajima, T., and M. Tanaka, 1986: Matrix formulation for the transfer of solar radiation in a plane-parallel scattering atmosphere, J. Quant. Spectrosc. Radiat. Transfer 35, 13–21.

Nakajima, T., and M. Tanaka, 1988: Algorithms for radiative intensity calculations in moderately thick atmospheres using a truncation approximation, J. Quant. Spectrosc. Radiat. Transfer 40, 51–69.

Nakajima, T., M. Tanaka, M. Yamano, M. Shiobara, K. Arao, and Y. Nakanishi, 1989: Aerosol optical characteristics in the yellow sand events observed in May, 1982 in Nagasaki—part II model, J. Meteorol. Soc. Jpn. 67, 279–291.

Omar, A. H., J.-G. Won, D. M. Winker, S.-C. Yoon, O. Dubovik, and M. P. McCormick, 2005: Development of global aerosol models using cluster analysis of Aerosol Robotic Network (AERONET) measurements. *J. Geophys. Res.*, **110**, D10S14, doi:10.1029/2004JD004874.

Pollack, J. B. and J. N. Cuzzi, 1980: Scattering by non-spherical particles of size

comparable to a wavelength: A new semi-empirical theory and its application to tropospheric aerosols. *J. Atmos. Sci.*, **37**, 868–881.

Rodgers, C. D., 2000, *Inverse Method for Atmospheric Sounding*, World Sci., Singapore, 240 pp.

Sayer, A. M., A. Smirnov, N. C. Hsu, and B. N. Holben, 2012: A pure marine aerosol model, for use in remote sensing applications. *J. Geophys. Res.*, **117**, D05213, doi:10.1029/2011JD016689.

Stamnes,K., S. C. Tsay, W. Wiscombe, and K. Jayaweera, 1988: Numerically stable algorithm for discrete-ordinate-method radiative transfer in multiple scattering and emitting layered media, Appl. Opt. 27, 2502–2509.

Tanaka, T. Y., and Chiba M.: Global simulation of dust aerosol with a chemical transport model, MASINGAR. J. Meteorol. Soc. Japan, 83A, 255–278, doi:10.2151/jmsj.83A.255, 2005.

Tanaka, T. Y., Orito, K., Sekiyama, T. T., Shibata, K., Chiba, M., and Tanaka, H.: MASINGAR, a global tropospheric aerosol chemical transport model coupled with MRI/JMA98 GCM: Model description, Pap. Meteorol. Geophys., 53, 119-138, 10.2467/mripapers.53.119, 2003.

Yoshida, M, M. Kikuchi, T. M. Nagao, H. Murakami, T. Nomaki, A. Higurashi,

Common retrieval of atmospheric aerosol properties for imaging satellite sensors, Journal of the Meteorological Society of Japan, 2018, doi:10.2151/jmsj. 2018-039.

Yoshida, M, K. Yumimoto, T. M. Nagao, T. Tanaka, M. Kikuchi, H. Murakami, Retrieval of Aerosol Combined with Assimilated Forecast, ACP, in review, 2020.

Yukimoto, S., Adachi, Y., Hosaka, M., Sakami, T., Yoshimura, H., Hirabara, M., Tanaka, T. Y., Shindo, E., Tsujino, H., Deushi, M., Mizuta, R., Yabu, S., Obata, A., Nakano, H., Koshiro, T., Ose, T., and Kitoh, A.: A new global climate model of the Meteorological Research Institute: MRI-CGCM3 – model description and basic performance, J. Meteorol. Soc. Japan, 90A, 23–64, doi:10.2151/jmsj.2012-A02, 2012.

Yumimoto, K., Tanaka, T., Yoshida, M, Kikuchi, M., Nagao, T. M., Murakami, and H., Maki, T.: Assimilation and Forecasting Experiment for Heavy Siberian Wildfire Smoke in May 2016 with Himawari-8 Aerosol Optical Thickness, Journal of the Meteorological Society of Japan, doi:10.2151/jmsj. 2018-035, 2018.